Modification of spontaneous emission rate in planar dielectric microcavity structures

Gunnar Björk
Department of Microwave Engineering, Royal Institute of Technology, S-100 44 Stockholm, Sweden

Susumu Machida, Yoshihisa Yamamoto, and Kazuhiro Igeta
NTT Basic Research Laboratories, Musashinoshi, Tokyo 180, Japan
(Received 22 August 1990)

The spontaneous emission rate and radiation pattern for a thin quantum well sheet enclosed by a one-dimensional dielectric microcavity have been calculated. By placing the sheet in the node (antinode) position of the cavity standing wave, the spontaneous emission in the direction normal to the sheet will be decreased (enhanced). In the former case the theory predicts that the spontaneous lifetime can be increased more than a factor of 10. In the latter case both theory and experiments confirm that such a simple structure can couple a substantial amount (30–90 %) of the spontaneous emission into the cavity resonant mode. In both cases, however, theory predicts that the spontaneous emission lifetime will increase for structures without guided modes.

I. INTRODUCTION

In 1946 Purcell[1] predicted that the spontaneous emission (SE) rate, and thus the relaxation lifetime of an excited atom, would be altered if the atom was put in a cavity with dimensions comparable to the transition wavelength. The reason for the modified SE rate is that spontaneous emission can be viewed as stimulated emission, stimulated by vacuum-field fluctuations. This view is the basis for this paper. The rate of spontaneous emission γ_{sp} is given by Fermi's golden rule:

$$\gamma_{sp} \equiv \frac{1}{\tau_{sp}} = \frac{2\pi}{\hbar} |\langle |\hat{\mathbf{d}}\cdot\hat{\mathbf{E}}^{\dagger}| \rangle|^2 \rho(\omega) , \tag{1}$$

where τ_{sp} is the spontaneous lifetime of the atom, $\hat{\mathbf{d}}$ is the material dipole operator, $\hat{\mathbf{E}}^{\dagger}$ is the electric-field creation operator at the location of the atom, and $\rho(\omega)$ is the density of optical modes per unit energy at the angular frequency ω. It is clear from Eq. (1) that the lifetime can be altered either by modifying the mode density, or by modifying the electric field at the location of the atom. In a microcavity both the mode density and the vacuum-field intensity will be different from those in free space or in a bulk sample. Since Purcell's early prediction, it has been shown experimentally, both in the microwave region,[2,3] and the optical region,[4–7] that the modification of the mode density and electric-field strength in a microcavity does indeed change the properties of the atom decay. In recent years several groups[7–9] have started to investigate how to fabricate microcavities in solid-state materials, using electron-hole pairs rather than excited atoms as a SE source. However, it has been an open question whether the cavity has to confine the waves in all three dimensions, or if a much simpler, planar structure can suffice. In this paper we show that a planar solid-state cavity structure, with cavity confinement in only one direction, will modify the SE decay of a thin sheet of electric dipoles noticeably.

II. SPONTANEOUS EMISSION IN A UNIFORM DIELECTRIC MEDIUM

Let us consider a two-level atom that has the transition frequency ω_0 and is located at $r = r_0$. We assume that the atom is initially in the excited state $|e\rangle$ while the field is in the vacuum state. The atom undergoes spontaneous decay to the ground state $|g\rangle$ by means of an electric dipole transition with the dipole moment $d = q\langle e|\hat{\mathbf{r}}|g\rangle$. We also assume that the interaction of the atom with the photon field is not too strong, so that the Weisskopf-Wigner theory of spontaneous emission[10] holds. Even when the atom is coupled with the microcavity internal field mode, the internal field dissipation is much stronger than the coherent coupling (vacuum-field Rabi flopping) between the field and the atom. Therefore, the spontaneous decay process proceeds exponentially.

The Hamiltonian of such a system is given by

$$\hat{H} = \hat{H}_A + \hat{H}_F + \hat{H}_{A\text{-}F} , \tag{2}$$

where the free-atom Hamiltonian is

$$\hat{H}_A = \hbar\omega_0 |e\rangle\langle e| , \tag{3}$$

and the free-field Hamiltonian is

$$\hat{H}_F = \sum_k \hbar\omega_k \hat{a}_k^{\dagger}\hat{a}_k . \tag{4}$$

The atom-field interaction Hamiltonian is

$$\hat{H}_{A\text{-}F} = -i\sum_k \left[\frac{\hbar\omega_k}{2}\right]^{1/2} \mathbf{d}\cdot\mathbf{f}_k(r_0)|e\rangle\langle g|\hat{a}_k + \text{H.c.} \tag{5}$$

Here $f_k(r)$ is the spatial-mode function with a wave vector k that obeys the eigenmode equations

$$\frac{\epsilon(r)\omega_k^2}{c_0^2}\mathbf{f}_k(r) - \nabla\times\nabla\times\mathbf{f}_k(r) = \mathbf{0} , \tag{6}$$

where c_0 is the speed of light in vacuum and ϵ is the

dielectric constant of the medium. The operator $|e\rangle\langle g|$ and its conjugate $|g\rangle\langle e|$ are the projection operators that represent the up and down electric dipole transitions.

The time-dependent solution of the Schrödinger equation for our system,

$$i\frac{d}{dt}|\Phi\rangle = H|\Phi\rangle \ , \tag{7}$$

can be written therefore in the form

$$|\Phi(t)\rangle = A(t)|1,\{0\}\rangle + \sum_k B_k(t)|0,1_k\rangle \ , \tag{8}$$

where $A(t)$ and $B_k(t)$ describe the probability amplitudes for the survival of an initial state and for emission of a single photon into the mode k. The amplitudes $A(t)$ and $B_k(t)$ obey the famous coupled differential equations and can be formulated by using the Laplace transform technique within the framework of the Weisskopf-Wigner approximation.[10] The solution for $A(t)$ is

$$A(t) = e^{-\gamma_{sp}t - i(\omega_0 + \Delta\omega_s)t}A(0) \ . \tag{9}$$

Here the spontaneous decay rate γ_{sp} is

$$\gamma_{sp} = \pi\sum_k \frac{\omega_k}{2\hbar}|\mathbf{d}\cdot\mathbf{f}_k(r_0)|^2\delta(\omega_k-\omega_0) \ , \tag{10}$$

while the radiative frequency shift $\Delta\omega_s$ is

$$\Delta\omega_s = -\sum_k \frac{\omega_k}{2\hbar}\mathrm{P}\frac{|\mathbf{d}\cdot\mathbf{f}_k(r_0)|^2}{(\omega_k-\omega_0)} \ . \tag{11}$$

P stands for the principal value.

If the atom is located within a uniform medium of relative dielectric constant ϵ, the local electric field the atom is subjected to is different from the macroscopic electric field.[11] By starting with the plane-wave solution, $\mathbf{f}_k(r) = [\hat{\mathbf{e}}_{k,\mu}/(\epsilon V)^{1/2}]e^{ikr}$, far away from the atom, and using a similar technique as when deriving the Clausius-Mossotti-Lorentz-Lorenz equation, we find that the mode function at the location of the atom is given by[11,12]

$$\mathbf{f}_k(r_0) = \frac{\hat{\mathbf{e}}_{k\mu}}{(\epsilon V)^{1/2}}\frac{3\epsilon}{2\epsilon+1} \ , \tag{12}$$

where $\hat{\mathbf{e}}_{k\mu}$ is a unit vector representing a polarization direction and V is the normalization volume. The last factor in (12) will henceforth be referred to as the local-field correction factor.

The mode summation in (10) is evaluated by noting that the mode density at frequency ω_k within the dielectric is $\rho(k) = (\epsilon^{3/2}\omega_k^2/\pi^2c_0^3)V$. The total decay rate is thus obtained as

$$\gamma_{sp} = \frac{2\pi}{\hbar}|\mathbf{d}\cdot\mathbf{f}_k(r_0)|^2\rho(k) = \frac{9\epsilon^{5/2}}{(2\epsilon+1)^2}\gamma_{sp}^{(free)} \ , \tag{13}$$

where $\gamma_{sp}^{(free)} = \omega_0^3 d^2/3\pi\hbar c_0^3$ is the spontaneous decay rate in free space. The probability of emitting a photon with the momentum k and polarization μ is given by

$$\gamma_{sp}(k,\mu,\omega_0) = \frac{9\epsilon^{5/2}}{(2\epsilon+1)^2}\frac{\omega_0^3}{\hbar c^3}\left[\frac{|\mathbf{d}\cdot\hat{\mathbf{e}}_{k\mu}|}{4\pi}\right]^2 . \tag{14}$$

Note that modification of γ_{sp} stems from the altered density of states, the altered global electric-field intensity, and from the local-electric-field intensity modification. In this paper we have concentrated on the former two effects.

For a sheet of dipole moments oriented such that $d_x^2 = d_y^2 = d^2/2$ and $d_z^2 = 0$, the probability of emitting a photon in S polarization is isotropic but that of emitting a photon in P polarization is proportional to $\cos^2\theta$, where θ is the emission angle measured from the z axis.

If the atom is located within a dielectric microcavity, the local electric field is no more related to a simple plane wave but rather it is modulated by multiple reflection effects. By assuming the plane wave, $\mathbf{f}_k(r) = [\hat{\mathbf{e}}_{k\mu}/(\epsilon V)^{1/2}]e^{ikr}$, incident from a semi-infinite uniform dielectric medium outside of the microcavity, we can calculate the local electric field by a transfer-matrix method that will be discussed next. The goal of the analysis in the following section is to study how the spontaneous lifetime $\tau_{sp} = 1/\gamma_{sp}$ and the radiation pattern are modified by the planar structured microcavity.

III. THEORETICAL MODEL

The structure is shown in Fig. 1. The cavity, which has an optical length of either one wavelength (λ cavity) or one-half wavelength ($\lambda/2$ cavity), is sandwiched between two dielectric mirrors. At the center of the cavity there is a thin planar quantum well. An excitonic transition in the quantum well (QW) is used as a SE source. The whole structure, including the mirrors, is surrounded by some bulk material extending in the normal direction to the interfaces for many, many wavelengths. In order to estimate the spontaneous emission rate we must calculate the electric field and the mode density at the location

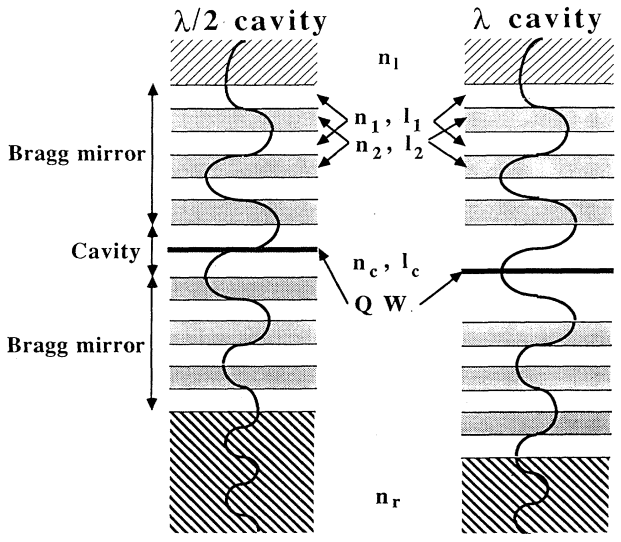

FIG. 1. A cross section of the planar microcavity structure. The cavity length is l_c, n_c is the refractive index of the cavity, and n_i and l_i ($i=1,2$) are the refractive index and the thickness of the respective layers. The refractive indices of the left- and right-hand-side bulk materials are n_l and n_r.

of the QW sheet. The planar cavity has been assumed to have infinite lateral dimensions. This is a reasonable model for the samples used in the experiments whose lateral dimensions were a few millimeters, which should be compared to the cavity length (a few hundred nanometers) and the wavelength (800 nm). The surrounding bulk material has been assumed to be infinitely thick. The conventional way of obtaining the mode density and the electric field in the microcavity is to surround it with a larger perfect cavity and solve the problem in the eigenmodes of the larger cavity. As the dimensions of the larger cavity tend to infinity the model will approach that of a microcavity surrounded by infinitely thick bulk material. However, the geometry of our microcavity does not lend itself easily to such an approach. We have opted for a different way to solve the problem. Our starting point has been to expand the incident vacuum-field modes in a plane-wave basis. This is, indeed, possible since plane waves constitute a complete orthogonal set. The vector potential and the electric field are described by a linear superposition of plane waves in the form[13]

$$\hat{\mathbf{A}}(r,t)=\sum_{k}\sum_{\mu=1}^{2}\left[\frac{\hbar}{2\omega_k\epsilon V}\right]^{1/2}\mathbf{e}_{k\mu}(\hat{a}_{k\mu}e^{ikr}+\hat{a}^{\dagger}_{k\mu}e^{-ikr}) , \tag{15}$$

$$\hat{\mathbf{E}}(r,t)=i\sum_{k}\sum_{\mu=1}^{2}\left[\frac{\hbar\omega k}{2\epsilon V}\right]^{1/2}\mathbf{e}_{k\mu}(\hat{a}_{k\mu}e^{ikr}-\hat{a}^{\dagger}_{k\mu}e^{-ikr}) . \tag{16}$$

For every wave we then calculate the enhancement or decrease of the electric field at the location of the QW sheet due to the cavity-mirror interference. We also take into account possible refraction of the wave. Thus, for every direction we can determine whether the cavity enhances or decreases the spontaneous emission into that mode. Summing the emission into the plane waves over all directions (i.e., **k** vectors), we can determine if the total emission is smaller or greater than, say, if the QW sheet were placed inside some specified bulk material.

In the calculation we can treat the vacuum-field operators $\hat{a}_{k\mu}$ and $\hat{a}^{\dagger}_{k\mu}$ classically, because the local field is expressed as a linear combination of those operators. When there is no product term of operators involved, the commutation relation $[\hat{a}_{k\mu},\hat{a}^{\dagger}_{k'\mu'}]=\delta_{kk'}\delta_{\mu\mu'}$ does not affect the result and the difference between quantum and classical analysis disappears. Of course, we need to evaluate the zero-point fluctuation intensity quantum mechanically for each incident plane wave. Expansion of the vacuum fields in coherent plane waves, and calculation of the local mean-square amplitude of the electric field is the very basis of our calculations.

To start our analysis we assume that in one of the two semi-infinite media surrounding the cavity mirrors both the mode density and the mean-square value of the vacuum-field fluctuations incident on the cavity are well defined and isotropic. Since the mode density is assumed to be isotropic in the medium, the plane waves must be isotropically distributed in **k** space. Since we do not quantize the modes, we cannot label them with a momentum quantization number. Instead, we identify each plane-wave mode by its angular frequency ω, its incidence angle θ, and its azimuthal angle φ. Thus, the number of modes per solid angle and unit energy in the medium $\rho(n,\omega)$ will not depend on the angle of incidence or azimuth, but only on the angular frequency, and possibly on the refractive index $n\equiv\epsilon^{1/2}$. However, in our calculation we have neglected the frequency dependence of ρ. This is a good approximation within the narrow frequency interval we are interested in. The incident waves from the medium are also all assumed to have a well-defined, angular independent electric-field mean-square value $\langle|\mathbf{E}(n)|^2\rangle$. We then go about to establish the relations between the mode densities and the mean-square values of the **E** fields incident from the two semi-infinite media. It will turn out that, in general, both the mean-square value of the **E** field and the mode density in the other medium will depend on θ. However, the product of the two will be independent of the incidence angle, as it should be in any isotropic medium. Finally, we use a transfer-matrix formalism to establish the relation between the **E** field at the QW position and the incident vacuum fields. This is done numerically, for every incidence angle, because a closed-form solution of this relation is very complicated in the general case. The price we pay for not rigorously quantizing the modes will now become apparent. We cannot quantitatively calculate the total spontaneous emission, we can only predict the spontaneous emission pattern, and we can accurately compute the ratio between the spontaneous lifetime in different structures.

In both the left- and right-hand side bulk dielectric there are left and right traveling waves (Fig. 2). We index, e.g., the right-traveling wave in the left-hand-side bulk material *rl*, and thus θ_l is the acute angle between the z axis and the k vector of that wave ($0\le\theta\le\pi/2$). In general θ changes as the plane wave propagates into a new slab. The incidence angle in slab i, θ_i, of a wave incident from the left-hand-side bulk is given by Snell's law,

$$\theta_i=\arcsin\left[\frac{n_l\sin(\theta_l)}{n_i}\right] , \tag{17}$$

where n_i and n_l are the complex refractive indices of slab i and the left-hand bulk material respectively, and θ_l is the incidence angle of the wave in the left-hand-side bulk. From this equation two things follow. First, due to cavity-mirror reflection the *ll* mode traveling in the

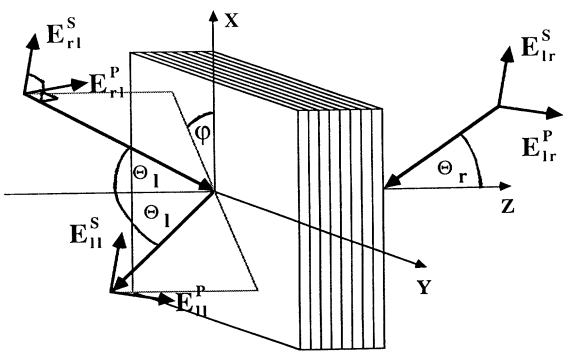

FIG. 2. Spherical coordinate system of the cavity structure.

(θ_l,φ) direction will in general couple both to the *rl* mode traveling in the $(\theta_l,\varphi+\pi)$ direction and the *lr* mode traveling in the

$$(\arcsin[n_l\sin(\theta_l)/n_r],\varphi+\pi)$$

direction. We have assumed that there is no correlation between the *rl* and *lr* modes. Second, since the propagation angle of a wave in any slab can be expressed in the left (or right) -hand-side bulk incidence angle we will use the incidence angle in the material with the highest refractive index as our incidence angle coordinate, and let it be a real number. Unless otherwise stated we will orient the structure such that $n_l \geq n_r$, and thus θ_l will be our incidence angle coordinate and will be a real number. It is clear from the equation that one must let θ_i be complex in order to be able to deal with complex refractive indices or evanescent waves.

Continuity of the **E** field across a dielectric boundary requires that the x and y components of the **k** vector of a plane wave be equal in all layers:

$$k_{ix}=k_{lx}=\frac{\omega n_l}{c_0}\sin(\theta_l)\cos(\varphi) , \tag{18}$$

$$k_{iy}=k_{ly}=\frac{\omega n_l}{c_0}\sin(\theta_l)\sin(\varphi) . \tag{19}$$

From the wave equation the z component of the **k** vector can be derived as

$$k_{iz}=\frac{\omega n_i}{c_0}\left[1-\left[\frac{n_l\sin(\theta_l)}{n_i}\right]^2\right]^{1/2} . \tag{20}$$

In the general case the **k** vector will be complex, too.

If the cavity or mirror refractive index is higher than both of the surrounding bulk refractive indices there is a possibility of having a guided mode, a mode that is propagating in the xy plane in the cavity (**k** is real) but is evanescent in the bulk materials (k_z is imaginary). Our model cannot cope with such structures since it assumes that all modes in the cavity couple to traveling waves in the surrounding media. This is an important limitation of the model and we ask the reader to note that although our model still will predict correctly the spatial distribution of the SE radiation, the SE lifetime cannot be calculated for any structure that supports guided modes. For our purposes this is not an important limitation, since a structure that supports guided modes cannot couple all of the emitted radiation into the direction normal to its surface, as we would like it.

The density of modes in slab i can be derived as follows. Suppose that N modes per unit energy propagate within the solid angle $d\Omega_l$ in the left-hand-side bulk material, so that

$$N=\rho(n_l)d\Omega_l=\rho(n_l)\sin(\theta_l)d\varphi\, d\theta_l . \tag{21}$$

From (17) it follows that in slab i these modes will propagate within a different solid angle given by

$$d\Omega_i=\sin(\theta_i)d\varphi\, d\theta_i=\sin(\theta_l)d\varphi\, d\theta_l\frac{n_l^2\cos(\theta_l)}{n_i^2\cos(\theta_i)}$$

$$=d\Omega_l\frac{n_l^2\cos(\theta_l)}{n_i^2\cos(\theta_i)} . \tag{22}$$

Using (17) and the trigonometric identity $\sin^2(\theta)+\cos^2(\theta)\equiv 1$, (22) can of course be expressed in θ_l only:

$$d\Omega_i=d\Omega_l\frac{n_l}{n_i}\left[\frac{1-\sin^2(\theta_l)}{(n_i/n_l)^2-\sin^2(\theta_l)}\right]^{1/2} . \tag{23}$$

Since the number of modes N within the two solid angles $d\Omega_l$ and $d\Omega_i$ are equal it follows that

$$\rho(n_l)d\Omega_l=\rho(n_i,\theta_i)d\Omega_i , \tag{24}$$

so that

$$\rho(n_i,\theta_i)=\rho(n_l)\frac{n_i^2\cos(\theta_i)}{n_l^2\cos(\theta_l)} , \tag{25}$$

where again θ_i can be expressed in θ_l by using (17). The mode density is a function of the refractive index n_i and the incidence angle θ_i, which is reasonable for a planar slab. Should index i denote the semi-infinite right-hand-side bulk material, (25) would seem to contradict our assumption that the right-hand-side bulk material is isotropic. As will be shown next, our choice of mode-density definition makes the mean-square expectation value of the **E** field in the right-hand-side bulk material have the inverse θ dependence so that the product of the two is angular independent.

Now we derive the relation between the mean-square expectation values of the vacuum fields incident from the left- and right-hand-side bulk materials. In general, a propagating wave will experience loss while propagating through a nonperfect dielectric. However, according to the definition our waves cannot lose any energy since they are in the vacuum state. What happens is that every mode couples to other vacuum-field modes via scattering. For an ideal linear lossy component the quantum-mechanical scattering relation between incident and outgoing modes reads

$$\hat{\mathbf{E}}_{\text{out}}=\sqrt{\exp(-\alpha L)}\hat{\mathbf{E}}_{\text{in}}+\sqrt{1-\exp(-\alpha L)}\hat{\mathbf{E}}_{\text{vac}} , \tag{26}$$

where α is the loss per unit length, L is the length of the component, and $\hat{\mathbf{E}}_{\text{vac}}$ is a vacuum-field-mode operator. For classical waves, the second term in (26) is absent. If the incident mode is in a vacuum state, the mean-square expectation value of the outgoing mode electric field will equal that of the incident mode due to the second term on the right-hand side (rhs) of (26). The second term will also ensure commutator bracket conservation. To include the scattering "loss" correctly in our theory we look at a planar infinite boundary between two dielectrics with refractive indices n_l and n_r, respectively. The z component (normal to the interface) of the Poynting vector **S** at a reference plane just to the left of the dielectric interface can be written

$$S_z=\frac{1}{2\omega\mu}\mathrm{Re}(k_{lz})(|E_{rl}^2-|E_{ll}|^2)+2\mathrm{Im}(k_{lz})\mathrm{Im}(E_{rl}^*E_{ll}) \quad (27)$$

for the S-polarized waves, and

$$S_z=\frac{1}{2\omega\mu}\mathrm{Re}\{(|E_{rl}|^2-|E_{ll}|^2+2jE_{rl}E_{ll}^*) \times[k_{lz}^*\cos(\theta_l)\cos^*(\theta_l) +k_{lx}\cos(\theta_l)\sin^*(\theta_l)]\} \quad (28)$$

for P-polarized waves, where Re and Im denote real and imaginary parts, μ is the permeability of the left-hand-side dielectric, and the asterisk denotes the complex conjugate. The left-going wave E_{ll} consists of two terms, a reflected wave and a transmitted wave. Using the Fresnel reflection formulas we obtain

$$E_{ll}=\frac{n_l\cos(\theta_l)-n_r\cos(\theta_r)}{n_l\cos(\theta_l)+n_r\cos(\theta_r)}E_{rl} +\frac{2n_r\cos(\theta_r)}{n_l\cos(\theta_l)+n_r\cos(\theta_r)}E_{lr} . \quad (29)$$

The wave incident from the right-hand-side bulk [(26)] can be written

$$E_{lr}=\sqrt{\exp(-j|\mathbf{k}_r|L)}E_0+\sqrt{1-\exp(-j|\mathbf{k}_r|L)}E_{\mathrm{vac}} , \quad (30)$$

where E_0 is the vacuum field incident from the right-hand-side bulk, a distance L along the propagation direction from the boundary. To derive the expression for E_{vac}, we assume that L is large enough to satisfy the relation $\exp(-J|\mathbf{k}_r|L)\ll 1$ so that the first term on the rhs of (30) vanishes. Combining (27), (29), and (30) we obtain

$$S_z=\frac{1}{\mu c_0}\left[\frac{n_l n_l^*\cos(\theta_l)\cos^*(\theta_l)\mathrm{Re}[n_r\cos(\theta_r)]}{|n_l\cos(\theta_l)+n_r\cos(\theta_r)|^2}|E_{rl}|^2-\frac{n_r n_r^*\cos(\theta_r)\cos^*(\theta_r)\mathrm{Re}[n_l\cos(\theta_l)]}{|n_l\cos(\theta_l)+n_r\cos(\theta_r)|^2}|E_{\mathrm{vac}}|^2\right] . \quad (31)$$

for an S-polarized wave. Since the vacuum fields cannot transport any energy along the direction normal to the dielectric interface, the time average of S_z must vanish and thus

$$\langle|E_{\mathrm{vac}}|^2\rangle=\frac{|n_l|^2|\cos(\theta_l)|^2\mathrm{Re}[n_r\cos(\theta_r)]}{|n_r|^2|\cos(\theta_r)|^2\mathrm{Re}[n_l\cos(\theta_l)]}\langle|E_{rl}|^2\rangle . \quad (32)$$

Doing the same algebra for the P-polarized wave one obtains

$$\langle|E_{\mathrm{vac}}|^2\rangle=\frac{|n_l|^2|\cos(\theta_l)|^2\mathrm{Re}[n_r^*\cos(\theta_r)]}{|n_r|^2|co(\theta_r)|^2\mathrm{Re}[n_l^*\cos(\theta_l)]}\langle|E_{rl}|^2\rangle . \quad (33)$$

The reason we obtain different results for S and P polarization in the general case is that if either or both n_l and n_r are complex, in general the waves can be planar only in one of the media. In the other medium the waves will be inhomogeneous and the S- and P-polarized beam simply no longer will be equal under rotational transformation. If both n_l and n_r are real (no losses) the waves will be planar in both bulk materials and the result will be the same for both polarizations and simplify to

$$\langle|E_{\mathrm{vac}}|^2\rangle=\frac{n_l|\cos(\theta_l)|^2\mathrm{Re}[\cos(\theta_r)]}{n_r|\cos(\theta_r)|^2\mathrm{Re}[\cos(\theta_l)]}\langle|E_{rl}|^2\rangle . \quad (34)$$

Now we are ready to check our results and to compare our expressions with those in Sec. II. We look at the planar interface between two semi-infinite bulk materials. Assume that the bulk materials have sufficiently small losses for their refractive indices to be assumed real, but that due to their infinite thicknesses, the first term on the rhs of (30) can be ignored, and the vacuum field incident towards the interface from the right-hand-side material can be expressed in that of the left-hand-side material through (34). The integrated mean-square electric field over a small solid angle $d\Omega_l$ in the left-hand-side material is $|\mathbf{E}_l^2\rho_l d\Omega_l$. Combining (25) and (34) the same quantity in the right-hand-side bulk is given by

$$|\mathbf{E}_{lr}|^2\rho_r d\Omega_r=\frac{n_l|\cos(\theta_l)|^2\mathrm{Re}[\cos(\theta_r)]}{n_r|\cos(\theta_r)|^2\cos(\theta_l)}|\mathbf{E}_{rl}|^2\frac{n_r^2\cos(\theta_r)}{n_l^2\cos(\theta_l)}\rho_l d\Omega_r = \begin{cases} n_r|\mathbf{E}_{rl}|^2\rho_l d\Omega_r/n_l & \text{if } n_l\sin(\theta_l)/n_r<1 \\ 0 & \text{if } n_l\sin(\theta_l)/n_r\geq 1. \end{cases} \quad (35)$$

It is clear that this result makes our theory consistent, as this product should be directionally independent for any isotropic bulk material. From (35) we can see that this is true as long as $n_r\leq n_l$ or θ_l is smaller than the critical angle. If θ_l is greater than the critical angle, plane-wave modes in the right-hand-side bulk coupling to the left-hand-side bulk modes with incident angle θ_l do not exist (so the waves incident from the left undergo total reflection at the boundary), and the result is zero. The factorization in (35) in the mode density and mean-square

field is somewhat arbitrary. These two factors always appear as a product in any bulk material; therefore, as pointed out in Ref. 14, one is free to choose which of the factors in (35) should be attributed to the mode density and which should be attributed to the incident vacuum fields. Comparing with the expressions in Sec. II one finds in a material with dielectric constant $\epsilon=n^2$ the corresponding product $|\mathbf{f}_k(r)|^2\rho(k)=\epsilon^{1/2}\omega_k^2/\pi^2c_0^3$, which is proportional to the refractive index of the material. This is in agreement with (35) above.

To calculate the electric field in the QW we have used numerical transfer-matrix multiplication.[15] The x, y, and time dependence of every mode are the same in every slab, as manifested by (18) and (19). The z-dependent part of the right- and left-hand-side traveling plane waves to the left of, e.g., a dielectric slab can be expressed in the corresponding waves to the right of the slab (Fig. 3). The simple transfer matrices for each slab are derived from Maxwell's equations.[16,17] Specifically, the matrix equation for a homogeneous planar dielectric, with its normal in the z direction, is

$$\begin{bmatrix} E_{rl} \\ E_{ll} \end{bmatrix} = \begin{bmatrix} \exp(jk_z\Delta z) & 0 \\ 0 & \exp(-jk_z\Delta z) \end{bmatrix} \begin{bmatrix} E_{rr} \\ E_{lr} \end{bmatrix}, \quad (36)$$

for both S- and P-polarization waves, if Δz is the distance between the two E-field reference planes. The matrix above depends on the incidence angle θ through (20) but is independent of φ due to the symmetry in the xy plane. This is true for every matrix equation due to the geometry. Thus, although we use all three dimensions in our theory, φ will not show up until we write down the expressions for the spontaneous emission rates. The transfer matrix for a planar interface between two dielectrics is (index 1 is that of the slab at the left)

$$\frac{1}{2}\begin{bmatrix} 1+\frac{k_{2z}}{k_{1z}} & 1-\frac{k_{2z}}{k_{1z}} \\ 1-\frac{k_{2z}}{k_{1z}} & 1+\frac{k_{2z}}{k_{1z}} \end{bmatrix}, \quad \frac{n_2}{2n_1}\begin{bmatrix} 1+\frac{n_1^2k_{2z}}{n_2^2k_{1z}} & 1-\frac{n_1^2k_{2z}}{n_2^2k_{1z}} \\ 1-\frac{n_1^2k_{2z}}{n_2^2k_{1z}} & 1+\frac{n_1^2k_{2z}}{n_2^2k_{1z}} \end{bmatrix} \quad (37)$$

for the S and P polarization, respectively. Chain multiplying the simple matrices (see Ref. 17), the relation between the waves at any two points in the structure can be obtained. Specifically, the relations between the waves in the QW layer and the incident waves can be written

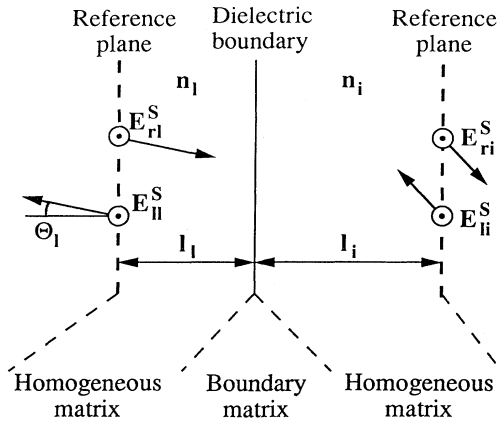

FIG. 3. Matrix representation of the structure. The right- and left-traveling waves at the left reference plane in the structure are labeled E_{rl} and E_{ll}, respectively. The total transfer matrix between the two reference planes is the product of the three matrices indicated in the figure.

$$E^s_{r\mathrm{QW}}(\theta)=\frac{B^s_{11}(\theta)}{AB^s_{11}(\theta)}E^s_{rl} + \left[B^s_{12}(\theta)-\frac{B^s_{11}(\theta)AB^s_{12}(\theta)}{AB^s_{11}(\theta)}\right]E^s_{lr} \quad (38)$$

and

$$E^s_{l\mathrm{QW}}(\theta)=\frac{B^s_{21}(\theta)}{AB^s_{11}(\theta)}E^s_{rl} + \left[B^s_{22}(\theta)-\frac{B^s_{21}(\theta)AB^s_{12}(\theta)}{AB^s_{11}(\theta)}\right]E^s_{lr}, \quad (39)$$

where the index s denotes field strengths and transfer matrices for S-polarized waves, A and B are the complex 2×2 transfer matrices representing all the dielectric slabs to the left- and right-hand sides of the quantum well, respectively, and $AB=A\times B$ is the matrix of the whole structure. Letting $s\rightarrow p$, the equations look identical for P-polarized waves.

The rate of spontaneous emission γ can now be calculated using (1), (17), (25), (34), (38), and (39). The emission rate due to the S-polarized vacuum-field fluctuations incident from the left-hand-side bulk per solid angle $d\Omega_l$ can be expressed

$$\gamma^s_l(\theta_l,\varphi)=\left|\frac{B^s_{11}(\theta_l)+B^s_{21}(\theta_l)}{AB^s_{11}(\theta_l)}\right|^2[d_x^2\sin^2(\varphi)+d_y^2\cos^2(\varphi)]\rho_0 n_l E_0^2\eta\left[\frac{3n_{\mathrm{QW}}^2}{2n_{\mathrm{QW}}^2+1}\right]^2, \quad (40)$$

where η is a constant, n_{QW} is the refractive index of the quantum well, d_x is the x component of the atom (or exciton) dipole moment, etc., and the last factor is due to the fact that the field the atom "senses" is different from the plane-wave superposition field [see Eq. (12)]. The rate due to the P-polarized wave reads

$$\gamma_l^p(\theta_l,\varphi)=\left[\left|\frac{B_{11}^p(\theta_l)-B_{21}^p(\theta_l)}{AB_{11}^p(\theta_l)}\right|^2[d_x^2\cos^2(\varphi)+d_y^2\sin^2(\varphi)]|\cos(\theta_{\mathrm{QW}})|^2\right.$$
$$\left.+\left|\frac{B_{11}^p(\theta_l)+B_{21}^p(\theta_l)}{AB_{11}^p(\theta_l)}\right|^2 d_z^2|\sin(\theta_{\mathrm{QW}})|^2\right]\rho_0 n_l E_0^2\eta\left[\frac{3n_{\mathrm{QW}}^2}{2n_{\mathrm{QW}}^2+1}\right]^2 \tag{41}$$

where θ_{QW} is the incidence angle in the QW layer. To calculate the SE rate due to the vacuum-field fluctuations incident from the right-hand side we use (34). The S-polarization rate reads

$$\gamma_r^s(\theta_l,\varphi)=\left|B_{12}^s(\theta_l)+B_{22}^s(\theta_l)-[B_{21}^s(\theta_l)+B_{11}^s(\theta_l)]\frac{AB_{12}^s(\theta_l)}{AB_{11}^s(\theta_l)}\right|^2[d_x^2\sin^2(\varphi)+d_y^2\cos^2(\varphi)]$$
$$\times\rho_0\frac{n_l^2\cos(\theta_l)\mathrm{Re}[\cos(\theta_r)]}{n_r\cos^2(\theta_r)}E_0^2\eta\left[\frac{3n_{\mathrm{QW}}^2}{2n_{\mathrm{QW}}^2+1}\right]^2 \tag{42}$$

and the P-polarization rate is

$$\gamma_r^p(\theta_l,\varphi)=\left[\left|B_{12}^p(\theta_l)-B_{22}^p(\theta_l)+[B_{21}^p(\theta_l)-B_{11}^p(\theta_l)]\frac{AB_{12}^p(\theta_l)}{AB_{11}^p(\theta_l)}\right|^2[d_x^2\cos^2(\varphi)+d_y^2\sin^2(\varphi)]|\cos(\theta_{\mathrm{QW}})|^2\right.$$
$$\left.+\left|B_{12}^p(\theta_l)+B_{22}^p(\theta_l)-[B_{21}^p(\theta_l)+B_{11}^p(\theta_l)]\frac{AB_{12}^p(\theta_l)}{AB_{11}^p(\theta_l)}\right|^2 d_z^2|\sin(\theta_{\mathrm{QW}})|^2\right]$$
$$\times\rho_0\frac{n_l^2\cos(\theta_l)\mathrm{Re}[\cos(\theta_r)]}{n_r\cos^2(\theta_r)}E_0^2\eta\left[\frac{3n_{\mathrm{QW}}^2}{2n_{\mathrm{QW}}^2+1}\right]^2. \tag{43}$$

The SE lifetime can now be calculated. It is simply the inverse of the SE rate integrated over all solid angle:

$$\frac{1}{\tau_{\mathrm{sp}}}=\int_\Omega d\Omega(\gamma_l^s+\gamma_l^p+\gamma_r^s+\gamma_r^p)$$
$$=\int_0^{2\pi}d\varphi\int_0^{\pi/2}d\theta_l\sin(\theta_l)(\gamma_l^s+\gamma_l^p+\gamma_r^s+\gamma_r^p)\,. \tag{44}$$

This equation assumes that if the two surrounding bulk materials have different refractive indices, the largest refractive index material should be on the left-hand side. For a general structure the integrand is quite complicated (we always obtain it from numerical matrix-chain multiplication) so the integral is calculated most readily by using a computer. However, the SE rate for an atom or exciton embedded in a homogeneous bulk material can be calculated easily by noting that if $n_{\mathrm{QW}}=n_l=n_r=n_i$ for all i, then $\theta_l=\theta_{\mathrm{QW}}=\theta_r$, $B_{12}^s=B_{21}^s=AB_{12}^s=0$, and $|B_{11}^s/AB_{11}^s|=|B_{22}^s|=1$, and similarly for the P-polarization matrices. From this it follows that $\gamma_l^s=\gamma_r^s$ and $\gamma_l^p=\gamma_r^p$, which is of course expected from the symmetry. One finds that the SE lifetime for an atom (or exciton) in a bulk material with refractive index n will be

$$\tau_{\mathrm{sp},0}=\frac{(2n_{\mathrm{QW}}^2+1)^2}{24\pi\eta\rho_0 n_{\mathrm{QW}}^5E_0^2(d_x^2+d_y^2+d_z^2)}\,. \tag{45}$$

The last thing to calculate is the far-field SE intensity. Our starting point has been to look at spontaneous emission as emission stimulated by vacuum-field fluctuations. Each emitted photon will be emitted in the form of dipole radiation, phase coherent with the stimulating electric field at the atom. The phase and the amplitude of the wave function of an emitted photon from one atom will be equal thus at any two points located at equal distances along a line through the atom. For a collection of atoms located randomly in a bulk material this means that the far-field SE radiation stimulated by a plane wave will be a plane wave in the forward direction where all the wave functions of the individual emission events add constructively, and zero in all other directions, where the phase relations are random, due to the random distribution of atoms. In a thin film (much thinner than a wavelength), however, the wave functions add constructively both in the forward (k_x,k_y,k_z) and the reflection $(k_x,k_y,-k_z)$ directions. The far field of the spontaneous emission will be two plane waves with equal magnitudes and phases traveling in the directions given above. This has recently been demonstrated by an interferometric measurement.[18]

Since the emitted spontaneous emission has this particularly simple form, symmetrically (both in phase and amplitude) emitted plane waves, it is easy to calculate the ratio of the emission leaving the left mirror to the total spontaneous emission. Using reciprocity one obtains the ratio ξ_l^s of the spontaneous emission leaving the left mirror in the θ_l direction, due to S-polarized vacuum-fields as

$$\xi_{ll}^s=\left[1+\left|\frac{(B_{12}^2+B_{22}^s)AB_{11}^s-(B_{11}^s+B_{21}^s)AB_{12}^s}{B_{11}^s+B_{21}^s}\right|^2\right.$$
$$\left.\times\frac{n_r\mathrm{Re}[\cos(\theta_r)]}{n_l\cos(\theta_l)}\right]^{-1}. \tag{46}$$

For a lossless structure the ratio of SE stimulated by the same polarization, leaving the right mirror in the θ_r direction, is $\xi_r^s=1-\xi_l^s$. For the P polarization the same

result holds, provided that $s \rightarrow p$ in the equations above, and that $d_x = d_y = d_z$.

IV. NUMERICAL RESULTS

We have used the theory outlined above to calculate the SE radiation pattern and the SE lifetime reduction or enhancement mainly for two different cavity structures. To maximize the SE radiation, we put the QW sheet at the antinode position of the cavity standing wave. To minimize the radiation, and thus prolong the SE lifetime, we propose to put the QW sheet at the node position instead. In both cases the cavity may be either a $\lambda/2$ cavity or a λ cavity, depending on the reflection phase of the Bragg mirrors (which in turn depends on the stacking order of the high and low refractive index slabs).

When the cavity length is of the order of a wavelength, the free spectral range for optical wavelengths is so great that a typical exciton transition linewidth is narrower than the cavity resonance linewidth, even if the cavity mirrors are highly reflecting. Thus, we only have to worry about one longitudinal mode, since no spontaneous emission will be emitted at wavelengths other than the resonant wavelength. In fact, although the exciton transition linewidth is finite, in the following calculations we have assumed a monochromatic SE source. This is a good approximation as long as the cavity resonance linewidth is much greater than the exciton transition bandwidth.

To simplify the presentation, and reduce to the number of degrees of freedom, we have assumed only two different refractive indices in the structure. In the enhancement λ cavity, n_l, n_r, n_1, and n_c all have been supposed to have the same, higher refractive index and n_2 has a lower index (Fig. 1). Choosing the refractive indices that way, there will be standing-wave antinodes both at the cavity-to-mirror interfaces, and in the center of the cavity. In the enhancement $\lambda/2$ cavity, n_l, n_r, and n_2 have been assumed to have the same, higher refractive index, and n_1 and n_c have the same lower index. The enhancement $\lambda/2$ cavity thus will have standing-wave nodes at the cavity-to-mirror interfaces and an antinode in the center of the cavity. In the suppression $\lambda/2$ cavity n_l, n_r, n_1, and n_c have the higher refractive index and n_2 has the lower refractive index. This structure will have a standing-wave node in the center of the cavity. Finally, we have done some calculations on a structure with a $\lambda/4$ long cavity where n_l, n_r, n_c, and n_2 have a high refractive index and n_1 has a lower index. This structure represents a continuous Bragg reflector with a QW sheet placed in its center.

In Fig. 4(a) the normalized radiation intensity of a quantum-well layer located at the center of an enhancement $\lambda/2$ cavity has been plotted as a function of θ_l. The dipoles in the QW layer have been assumed to be oriented within the QW plane ($d_z = 0$). This radiation pattern can be compared to that of the same dipole sheet sitting in a transparent bulk material with the same refractive index as the QW. This curve (dotted) drops from unity at normal incidence to one-half at grazing incidence. The reason for this is that since electric dipoles only interact with the electric-field component parallel to the dipole orientation, a collection of dipoles with their dipole moments oriented in a plane will only interact with the *S*-polarization waves at grazing incidence, whereas both polarizations will interact at normal incidence.

Four distinct regions can be seen in the plot: Close to 0° (normal incidence) the spontaneous emission is greatly enhanced due to the cavity resonance. For slightly larger angles there is a region where the spontaneous emission is suppressed. This is due to the stopbands at each side of the resonant window of the Bragg reflector cavity structure. The incident vacuum fields are reflected from the structure and the field strength decays exponentially as a function of mirror penetration depth. Inside the cavity almost no electric field exists. At even greater incidence angles, the Bragg reflectors are virtually transparent due to the mismatch between the period length seen from this angle, and the SE wavelength, and the radiation intensity oscillates around its "bulk value." For angles greater than $\theta_c = \arcsin(n_2/n_l)$ one would expect a very fast decay in the SE intensity since the incident waves propaga-

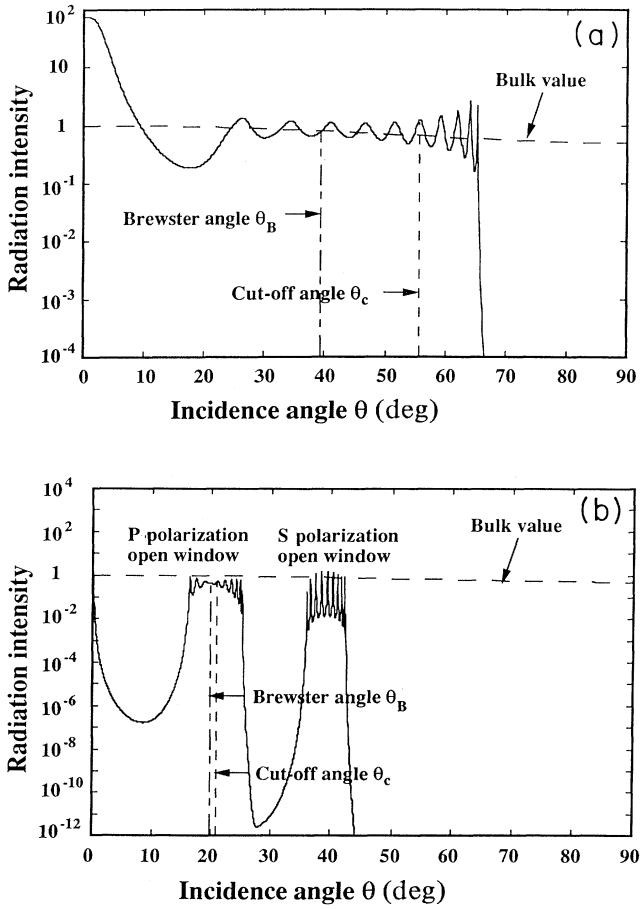

FIG. 4. Spontaneous intensity radiation pattern as a function of incident angle for an enhancement $\lambda/2$ cavity with the dipoles oriented in the plane of the quantum well. In (a) $n_l = n_r = n_2 = 3.6$, and $n_1 = n_c = 2.96$. In (b) n_1 and n_c are equal to 1.3.

ting through the n_2 refractive index layers are evanescent. As can be seen from the figure, however, the waves will propagate through the structure through resonant tunneling in a band extending well beyond θ_c. It turns out that this larger observed cutoff angle is approximately given by $\arcsin(n_m/n_l)$ where $n_m=(n_1+n_2)/2$.

For a larger refractive index difference, the figure looks similar, but more pronounced [Fig. 4(b)]. The SE intensity close to zero will increase enormously (the value at $\theta=0$ is around 46×10^6), and the "open window" will split into two. The window closer to zero incidence will be that of the P polarization. It will always be centered around the Brewster angle $\theta_B=\arctan(n_2/n_1)$ where the Bragg mirrors are transparent for the P-polarization waves. The open window for the S polarization is found just below $\theta=\arcsin(n_m/n_l)$ due to the resonant tunneling mentioned above. The reflectivity of the Bragg mirrors will rapidly oscillate between near zero to a few percent from unity within this window. However, since the waves are evanescent inside the cavity, both the wave penetrating the left mirror and right mirror will decay exponentially as they propagate toward the QW layer. Since the QW layer is placed in the center of the cavity it will always be at the minimum of the total electric field. Thus, the spontaneous emission will not be enhanced even though there will be substantial standing waves in the Bragg mirrors at a number of incidence angles within the open window.

Increasing the number of layers of alternating high and low refractive index material in the Bragg mirror, the SE intensity close to zero incidence angle will increase. At the same time the peak will get narrower. The SE intensity integrated over the solid angle within the cavity passband and stop band will remain virtually constant. The number of layers in the Bragg reflectors thus will not affect the SE lifetime, only the radiation pattern will be altered.

In Fig. 5 the radiation intensity for a supression-type $\lambda/2$ cavity has been plotted. It is similar to that shown in Fig. 4(a) except close to zero incidence where the emission is suppressed instead of enhanced.

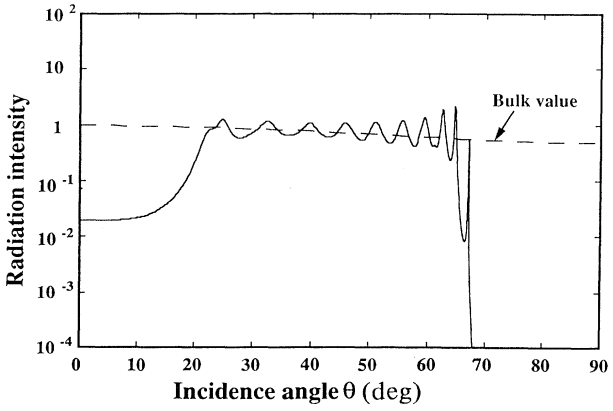

FIG. 5. Spontaneous intensity radiation pattern as a function of incident angle for a suppression $\lambda/2$ cavity with the dipoles oriented in the plane of the quantum well. The parameters are $n_l=n_r=n_1=n_c=3.6$, $n_2=2.96$.

The efficiency with which the spontaneous emission is emitted into the cavity resonant "mode" is calculated as

$$\beta=\frac{\int_0^{2\pi}d\varphi\int_0^{\theta_0}\sin(\theta)d\theta(\gamma_l^s+\gamma_l^p+\gamma_r^s+\gamma_r^p)}{\int_0^{2\pi}d\varphi\int_0^{\pi/2}\sin(\theta)d\theta(\gamma_l^s+\gamma_l^p+\gamma_r^s+\gamma_r^p)}\ . \quad (47)$$

Here θ_0 is the angular spread of the cavity resonant "mode," defined as the angle at the first minimum of the SE radiation intensity. Since the structure does not support any guided modes the definition of θ_0 is of course quite arbitrary. When looking at the radiation intensity in a polar coordinate system, our choice will seem quite natural. It is important to bear in mind though that what we call the cavity resonant "mode" is not a true mode. Since our one-dimensional structure does not have any lateral mode confinement and no preferred polarization direction, the obtained radiation intensity is the effect of the superposition of many modes. In practice one would like to reduce those to one, or at most a few. That could be achieved by a gain-guided structure or, as suggested in the accompanying paper,[19] by etching a cylindrical post in the planar chip. In Fig. 6(a) the coupling efficiency is

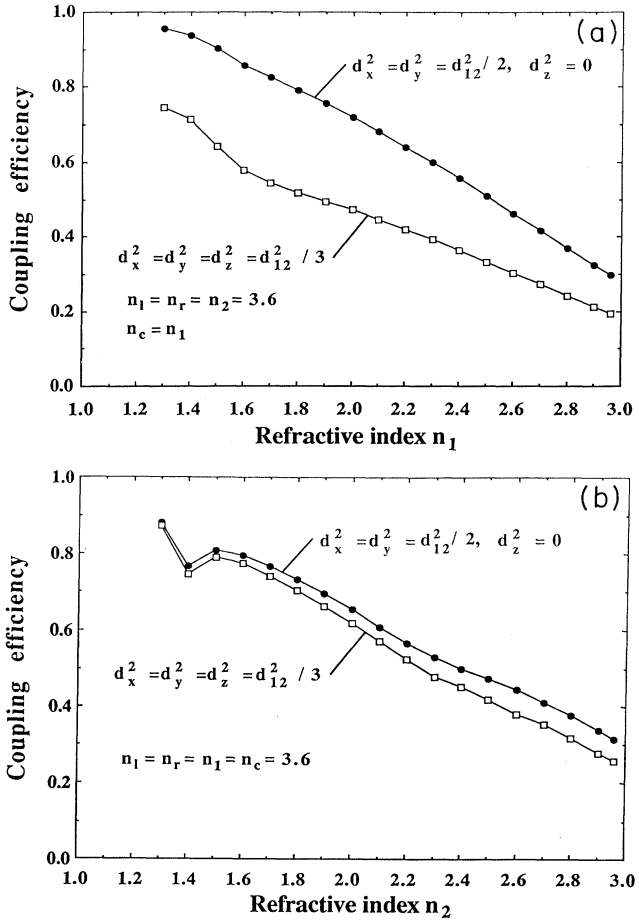

FIG. 6. Coupling efficiency of spontaneous emission coupling into the cavity resonant "mode" vs refractive index of the Bragg mirror layer with lowest refractive index. In (a) the cavity is half a wavelength long; in (b) one wavelength long. The dipole strength in the i direction is denoted d_i.

plotted for an enhancement $\lambda/2$ cavity. It can be seen that it increases from around 30% for $n_2=2.96$ to over 90% when $n_2=1.3$. (The end point $n_2=1.3$ for the calculations was chosen rather arbitrarily. However, it is difficult to think of an optically suitable solid-state material with even lower refractive index.) It is also clear from the figure that the coupling efficiency is higher for a structure where the electric dipoles lie oriented only in the QW plane than if they are randomly oriented. In Fig. 6(b) the same calculation has been done for an enhancement λ cavity. The coupling efficiency is slightly lower, but again the coupling efficiency goes towards unity with increasing refractive index (decreasing n_1).

The SE lifetime ratio $\tau_{sp}/\tau_{sp,0}$ can be calculated from (44) and (45). In Fig. 7(a) the ratio between the SE lifetime of an exciton sheet placed in an enhancement $\lambda/2$ cavity and the reference SE lifetime for the *same* exciton sheet located in a transparent bulk material with a refractive index of 3.6 is plotted versus n_1. Please note that since $n_{QW}=3.6$ has been the same in all the cavity structures and the reference structure, the local field-correction factors have canceled in calculating the SE lifetime ratio. Contrary to what one would expect from such a "leaky" structure (which has cavity confinement in only one direction), the lifetime of the excitons in the cavity is *longer* than if the excitons were placed without mirrors surrounded by the bulk material. This is due to the fact that within the cavity passband and stop band, the radiation intensity pattern is approximately a redistribution of the vacuum-field fluctuations within that solid angle. Outside the cavity stop band, the structure has a passband for each polarization, but is otherwise highly reflecting. In the passband region the vacuum-field fluctuations at the QW layer are roughly equal to those in the surrounding bulk material. In the reflection regions the vacuum field does not penetrate the Bragg mirrors all the way to the QW layer and cannot stimulate the excitons to decay. These "dark" regions will cause the excitons to live longer. In Fig. 7(b) the same calculation is done for a λ cavity. Here the increase of the lifetime is even more pronounced. However, if one's goal is to extend the SE lifetime one should of course put the QW plane in a node

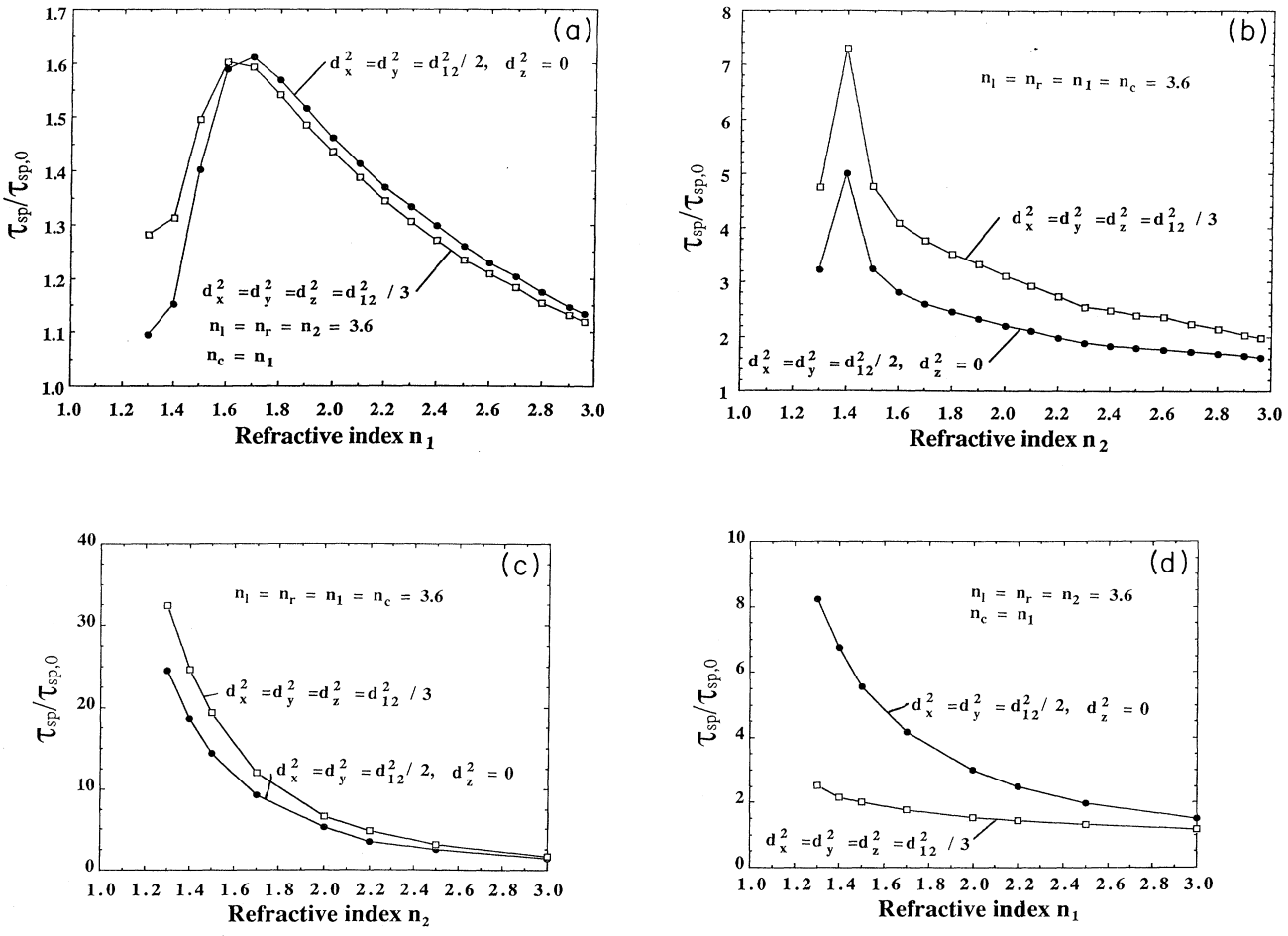

FIG. 7. Spontaneous emission lifetime ratio, $\tau_{sp}/\tau_{sp,0}$, vs refractive index of the Bragg mirror layer with lowest refractive index. The cavities in the different plots are (a) $\lambda/2$, enhancement type; (b) λ, enhancement type; (c) $\lambda/2$, suppression type; (d) $\lambda/4$, suppression type. The dipole strength in the i direction is denoted d_i.

position of the cavity standing wave. In Fig. 7(c) we have used the suppression-type $\lambda/2$ cavity in the calculation yielding even longer SE lifetimes. Note, however, that it is important that the QW is thin and accurately centered in the cavity since the standing wave has a spatially quite sharp minimum. In this calculation we assumed a 80-Å-thick QW. Finally, in Fig. 7(d) we have calculated the lifetime ratio for a continuous Bragg reflector with a QW centered in its middle. The "forbidden gap" in such a reflector at the Bragg wavelength causes the lifetimes to increase, but the effect is smaller than with the previous cavity type. It is interesting to note that it makes quite a difference whether the dipole moments are oriented in a plane or if they are isotropically oriented. This has to do with the fact that the d_z dipole moment only interacts with the P-polarized waves for which the grating is transparent close to the Brewster angle.

V. EXPERIMENTAL RESULTS

The structures we have used are similar to those in Fig. 1, although not perfectly symmetric. The $Al_{0.2}Ga_{0.8}As$ cavity (n_c), which has an optical length of either one wavelength (λ cavity) or one-half wavelength ($\lambda/2$ cavity) is sandwiched between two dielectric mirrors each made by 20 alternating layers of $Al_{0.2}Ga_{0.8}As$ (n_1) and AlAs (n_2). The λ cavity has two quantum wells, each positioned 4 nm from the cavity center (antinode position) of the cavity and is predicted to have an enhanced SE rate at the resonant wavelength. The $\lambda/2$-cavity sample also has two quantum wells, each positioned 4 nm from the cavity center (node position), and is expected to have a reduced SE rate. In addition, we have measured the SE radiation of a single planar QW sheet embedded deep into a many, many wavelengths-thick slab of $Al_{0.2}Ga_{0.8}As$. The GaAs quantum wells have a narrow linewidth (5 Å) excitonic transition at 800 nm which is used as a SE source. The excitonic dipoles formed by the lowest-conduction electrons and the lowest heavy holes can be considered oriented in the QW plane as the dipole strength in the x and y directions are about an order of magnitude greater than that in the z direction, at moderate excitations. The whole structure is grown by molecular-beam epitaxy on a GaAs substrate (n_r).

Both samples were grown with tapered layer thicknesses. Thus the cavity resonant wavelength varied along the length of the samples, while the exciton transition wavelength was kept constant throughout each sample. Then rotating the Dewar bottle, three Ar-laser "pointer" beams were used to assure that the center of rotation lay within the microcavity plane, not to translate accidentally the measurement point with respect to the pump-laser beam. At each measurement point the cavity structure reflectivity was measured using a white-light source. By translating the sample little by little, a point where the cavity resonant wavelength λ_0 and the exciton transition wavelength λ_e coincided could be found easily.

While measuring the spontaneous emission, all samples were optically pumped by a tunable Ti-sapphire laser, and the spontaneous emission was passed through a monochrometer and detected by a photomultiplier. The

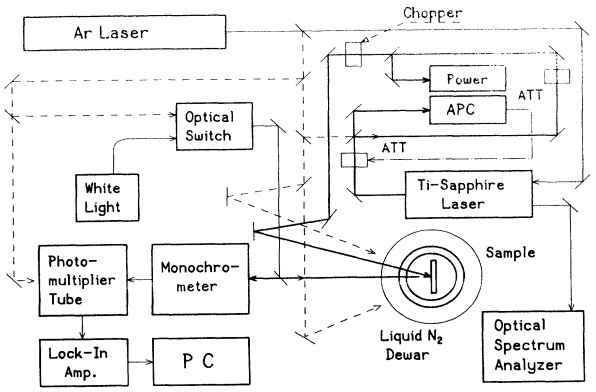

FIG. 8. Measurement setup. The automatic power controller (APC) keeps the pump-light intensity constant by regulating the attenuator (ATT).

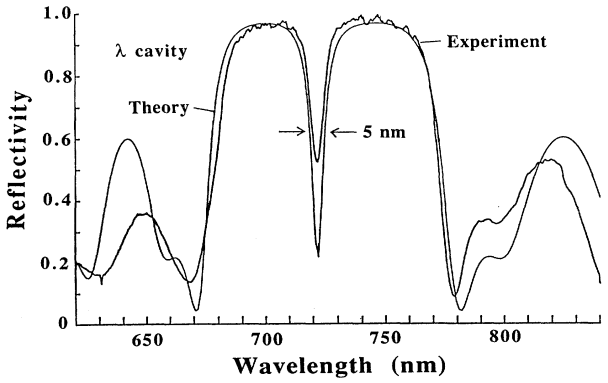

FIG. 9. Measured and calculated cavity reflectivity.

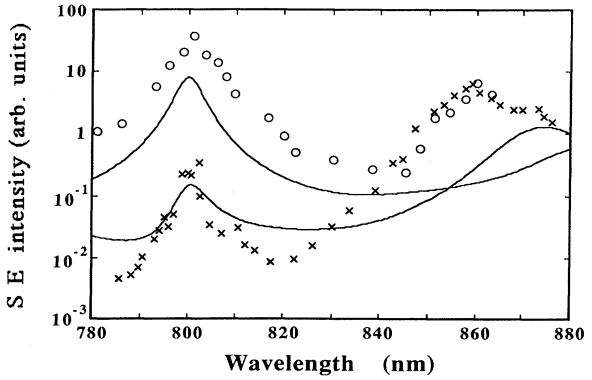

FIG. 10. Calculated and measured spontaneous emission intensity in the normal direction.

samples were cooled in liquid nitrogen ($n_l \simeq 1.48$) to reduce the emission linewidth and the Auger recombination. Since the spontaneous emission increased linearly with the pump intensity within the 1-μW to 1-mW pump power range and with the pump beam spot size of 100 μm, we have a good indication that spontaneous emission is the dominant recombination process and that the stimulated emission is negligibly small. The measurement setup is shown in Fig. 8.

The limited size of the Dewar-bottle window allowed measurements only between $\pm 65°$. Due to the low refractive index of the liquid nitrogen this corresponds to only $\pm 22°$ in the GaAs quantum well. Thus only the strong central lobe and the surrounding stop band could be seen.

In Fig. 9 the measured and calculated reflectivity of the λ-cavity sample is plotted, showing a reasonable agreement between the two curves. The theoretical curve assumes a perfect sample and is drawn using only two fitting parameters (period length and $Al_{0.2}Ga_{0.8}As$ refractive index). In Fig. 10 the measured and calculated spontaneous emission intensity in the normal direction is shown. On resonance, the λ cavity (top curve, circles) shows a substantial enhancement of the SE intensity, while the $\lambda/2$ cavity (bottom curve, crosses) features a reduced SE intensity just off resonance. Had the $\lambda/2$ cavity instead had only one thin quantum well, centered in the cavity, the SE would have been inhibited just at the resonant wavelength. In the figure, we have attempted to draw the experimental points from the two samples using the same normalization factor; however, due to the fact that the samples have different QW layers the ordinates for the two different samples may not coincide. The theoretical curve assumes identical dipole moment strengths.

The radiation pattern measurements also agreed qualitatively with theory. The sample without any mirrors had nearly constant radiation intensities for *s* and *p* polarizations within the measurement window, as shown in Figs. 11(a) and 11(b). (The angles in Fig. 11 are those in the GaAs substrate.) The λ cavity showed a pronounced

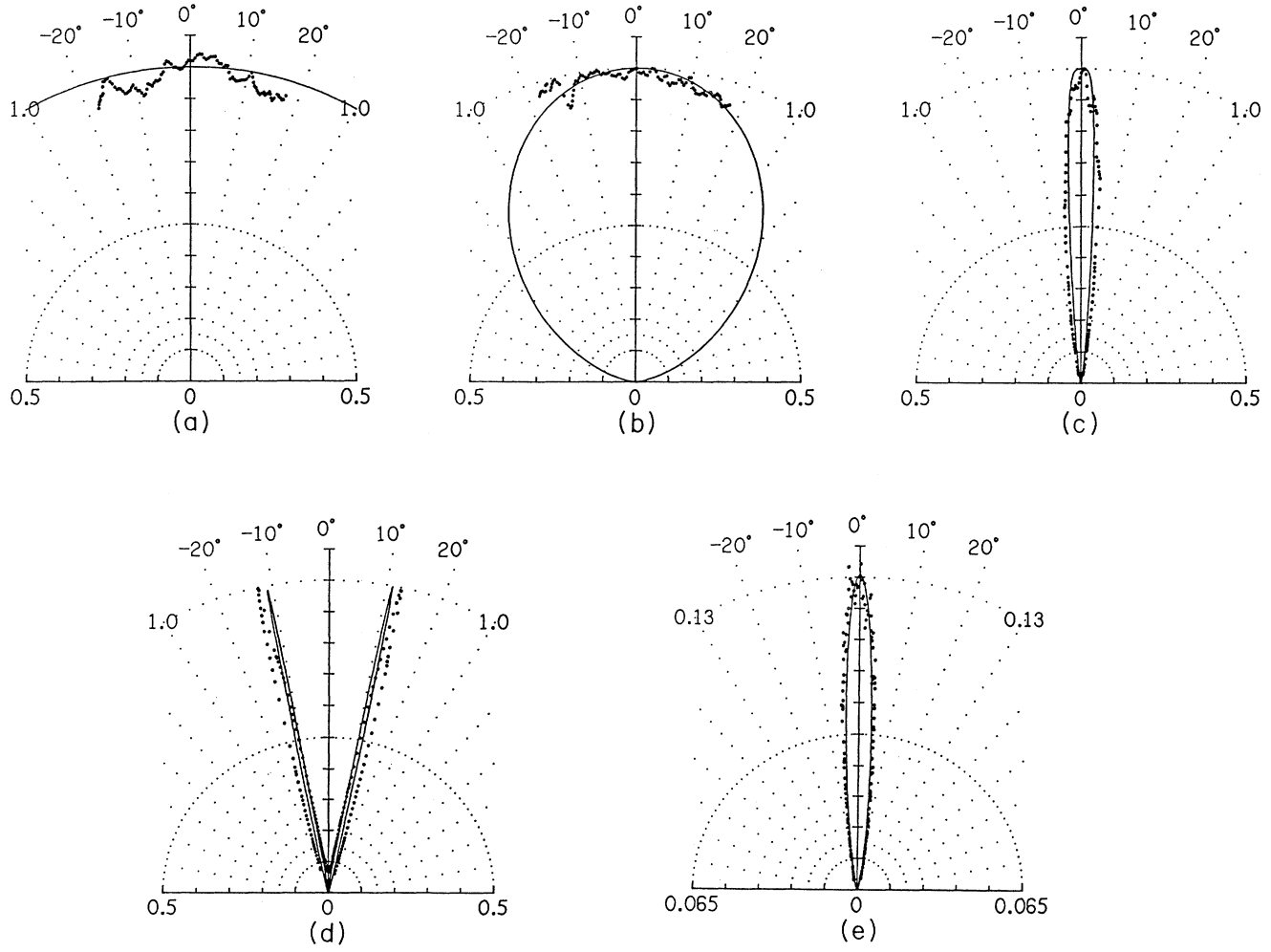

FIG. 11. The experimental and theoretical radiation patterns from the GaAs quantum well. (a) a thick $Al_{0.2}Ga_{0.8}As$ layer (*s* wave); (b) a thick $Al_{0.2}Ga_{0.8}As$ layer (*p* wave); (c) a λ cavity ($\lambda_e = \lambda_0 = 800$ nm); (d) a λ cavity ($\lambda_e = 800$ nm, $\lambda_0 = 815$ nm); (e) a λ cavity ($\lambda_e = 800$ nm, $\lambda_0 = 790$ nm).

central lobe with a 3-dB dropoff limit at $\pm 4°$ as shown in Fig. 11(c) when the cavity resonant wavelength and the emission wavelength are coincident. This agrees well with theory [see Fig. 4(a) also]. When the emission wavelength λ_e is shorter than the cavity resonant wavelength λ_0, a conical emission pattern is observed, as shown in Fig. 11(d). The emission angle of 12° agrees well with the theoretical resonance angle, $\theta_r = \cos^{-1}(\lambda_e/\lambda_0) \simeq 11°$. On the other hand, when λ_e is longer than λ_0, a simply attenuated single peak centered at $\theta = 0$ is observed, as shown in Fig. 11(e). This is because the cavity resonance condition is not satisfied by any angle for $\lambda_e > \lambda_0$.

VI. CONCLUSIONS

It has been shown theoretically that both the spontaneous emission lifetime and the radiation pattern can be modified by placing an excited atom or an exciton in the center of a planar dielectric cavity. For the proposed structures the spontaneous emission lifetime will be longer than in bulk material, and the spontaneous emission will be concentrated to a rather narrow central lobe. This structure is promising because it is simple to fabricate by employing, e.g., molecular-beam epitaxy.

ACKNOWLEDGMENTS

The authors would like to thank Dr. Eli Yablonovitch for pointing out Ref. 17 to us. One of us (G.B.) would also like to thank NTT for inviting him to participate in this project.

[1] E. M. Purcell, Phys. Rev. **69**, 681 (1946).
[2] P. Goy, J. M. Raimond, M. Gross, and S. Haroche, Phys. Rev. Lett. **50**, 1903 (1983).
[3] P. Filipovicz, P. Meystre, G. Rempe, and H. Walther, Opt. Acta **32**, 1105 (1985).
[4] K. H. Drexhage, in *Progress in Optics,* edited by E. Wolf (North-Holland, Amsterdam, 1974), Vol. XII, p. 165.
[5] F. De Martini, G. Innocenti, G. G. Jacobovitz, and P. Mataloni, Phys. Rev. Lett. **59**, 2955 (1987).
[6] D. J. Heinzen, J. J. Childs, J. E. Thomas, and M. S. Feld, Phys. Rev. Lett. **58**, 1320 (1987).
[7] H. Yokoyama, K. Nishi, T. Anan, and H. Yamada (unpublished).
[8] Y. Yamamoto, S. Machida, K. Igeta, and Y. Horikoshi, in *Coherence and Quantum Optics IV,* edited by L. Mandel, E. Wolf, and J. H. Eberly (Plenum, New York, 1990).
[9] E. Yablonovitch, T. J. Gmitter, and R. Bath, Phys. Rev. Lett. **61**, 2546 (1988).
[10] V. Weisskopf and E. Wigner, Z. Phys. **63**, 54 (1930).
[11] A. R. Von Hippel, *Dielectrics and Waves* (Wiley, New York, 1954).
[12] R. J. Glauber and M. Lewenstein (private communication).
[13] W. H. Louisell, *Radiation and Noise in Quantum Electronics* (McGraw-Hill, New York, 1964).
[14] S. D. Brorson, H. Yokoyama, and E. P. Ippen, J. Quantum Electron. **QE-26**, 1492 (1990).
[15] G. Björk and O. Nilsson, J. Lightwave Technol. **LT-5**, 140 (1987).
[16] M. Born and E. Wolf, *Principles of Optics,* 6th ed. (Pergamon, Oxford, 1980), p. 66.
[17] P. Yeh, *Optical Waves in Layered Media* (Wiley, New York, 1988), p. 102.
[18] M. Lai and J. C. Diels, Am. J. Phys. **58**, 928 (1990).
[19] Y. Yamamoto, S. Machida, and G. Björk, preceding paper, Phys. Rev. A **43**, 657 (1991).